

Log-periodic drift oscillations in self-similar billiards

Felipe Barra¹, Nikolai Chernov² and Thomas Gilbert³

¹ Departamento de Física, Facultad de Ciencias Físicas y Matemáticas, Universidad de Chile, Casilla 487-3, Santiago Chile

² Department of Mathematics, University of Alabama at Birmingham, Birmingham, AL 35294, USA

³ Center for Nonlinear Phenomena and Complex Systems, Université Libre de Bruxelles, CP 231, Campus Plaine, B-1050 Brussels, Belgium

E-mail: fbarra@dfi.uchile.cl, chernov@math.uab.edu and thomas.gilbert@ulb.ac.be

Received 17 May 2007, in final form 5 September 2007

Published 28 September 2007

Online at stacks.iop.org/Non/20/2539

Recommended by C P Dettmann

Abstract

We study a particle moving at unit speed in a self-similar Lorentz billiard channel. The latter consists of an infinite sequence of cells which are identical in shape but growing exponentially in size, from left to right. We present a numerical computation of the drift term in this system and establish the logarithmic periodicity of the corrections to the average drift.

PACS numbers: 05.45.–a, 05.70.Ln, 05.60.–k

(Some figures in this article are in colour only in the electronic version)

1. Introduction

Over the last few decades, the theory of hyperbolic dynamical systems has become the cornerstone in the foundation of non-equilibrium statistical mechanics. The interest in hyperbolic models stems from relations between macroscopic features characteristic of irreversible phenomena, such as entropy production or transport coefficients, and dynamical properties, such as Lyapunov exponents [1–4].

Billiard models, whose dynamics are conveniently described in terms of collision maps, have proved extremely useful in this regard [5]. The simplest example is the two-dimensional periodic Lorentz gas with finite horizon, which exhibits diffusion without a drift [6]. In a statistically stationary state, this model represents a mechanical system at equilibrium, whose distribution, measured along the boundary of the scattering discs, is uniform in the position and normal velocity angles. Meanwhile the process of relaxation to equilibrium itself is characterized by deterministic hydrodynamic modes of diffusion with fractal properties [7]. One can also induce a non-equilibrium stationary state on a cylindrical version of this billiard

by coupling it to stochastic reservoirs of point-particles at its boundaries [8]; these are the so-called flux boundary conditions. In this case, a difference between the chemical potentials of the reservoirs will transform to a linear gradient of density across the system, which is responsible for a steady current, given according to Fick's law of diffusion, and positivity of the entropy production, see [3].

Whereas the previous examples of billiards are Hamiltonian systems which preserve phase-space volumes, one can also consider dissipative periodic billiards driven out of equilibrium by the action of an external field. Thus the Gaussian iso-kinetic periodic Lorentz gas is similar to the usual periodic Lorentz gas, but for the action of a thermostated uniform external field which bends the trajectories in the direction of the field while keeping the particle's kinetic energy constant [1]. This field therefore induces a non-equilibrium stationary state with which is associated a constant drift current, according to Ohm's law [9]. Moreover, due to the dissipation induced by the thermostat, phase-space volumes are, on average, contracted. Therefore the sum of the Lyapunov exponents is strictly negative in the presence of the field and one can in fact identify this sum as minus the entropy production rate [10].

Gaussian iso-kinetic dynamics are different from Hamiltonian dynamics in that the latter preserve the total energy, whereas the former preserve the kinetic energy. One can nevertheless describe the Gaussian iso-kinetic dynamics by a Hamiltonian formalism, as shown in [11]. A general theorem due to Wojtkowski [12] stipulates that Gaussian iso-kinetic trajectories are geodesic lines of the so-called torsion free connection (also known as the Weyl connection). The Gaussian iso-kinetic Lorentz gas can thus be conformally transformed into a distorted billiard table on which trajectories become straight lines; besides, the conformal transformation preserves the specular character of the collision laws [13]. Although the trajectories thus transformed no longer have constant speed, one can introduce, for any given trajectory, a time-reparametrization under which the speed does remain constant.

A volume-preserving billiard in a distorted channel is therefore a natural generalization of iso-kinetic dynamics in a field-driven Lorentz channel. Ignoring the strict periodicity of the latter billiard, one may put aside the problem of time scales altogether and consider the dynamics of independent point-particles moving at constant speed in the new geometry. The dynamics of the resulting billiard are thus strictly Hamiltonian and bear no immediate connection to the Gaussian iso-kinetic dynamics. Such self-similar billiard channels were introduced in [14, 15]; they consist of an infinite sequence of (non-identical) two-dimensional cells that are attached together and make a (non-uniform) one-dimensional channel. The cells are identical in shape, but their sizes are scaled by a common factor. As a particle moves from one cell to a neighbouring one, its velocity remains unchanged while the length scales are expanded (or contracted), so that the time scales between collisions change accordingly. A noticeable property of these billiards concerns their long-term statistics; even though their dynamics preserve phase-space volumes, their statistics are characterized by a non-equilibrium stationary state with fractal properties and a drift, quite similar to the Gaussian iso-kinetic Lorentz gas itself. Close to equilibrium (when the scaling between neighbouring cells is close to unity), one can relate the constant drift velocity to the diffusion coefficient of the equilibrium system, which is nothing but the usual Lorentz channel, see [15].

In a recent paper [16], Chernov and Dolgopyat unveiled a remarkable feature of the drift term of self-similar billiards, namely that the linear growth of the particles' displacements with respect to time is, on average, periodic on logarithmic time scales, or log-periodic, with a period specified by the scaling parameter. This term may therefore display periodic oscillations. The purpose of this paper is to establish this property and provide further insight into this peculiar phenomenon, which actually stems from the discrete scale invariance of self-similar billiards [17]. We will offer numerical evidence which demonstrates the existence

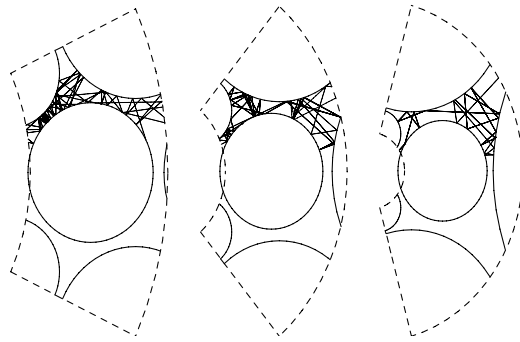


Figure 1. Three examples of unit cells with short trajectories. The parameter values (defined in the text) are, respectively, $\epsilon = 0.5$ and $\rho = 0.459\,738$ (left), $\epsilon = 1$ and $\rho = 0.440\,862$ (centre) and $\epsilon = 1.5$ and $\rho = 0.413\,317$ (right).

of log-periodic drift oscillations for self-similar billiards which are sufficiently far away from equilibrium. Closer to equilibrium these oscillations are, at least numerically, found to vanish. Thus, for all practical purposes, we may assume that the drift is constant close to equilibrium, and grows as a linear function of the scaling parameter. Further away from equilibrium, this linear dependence of the average drift in the scaling exponent is not expected to remain valid. In contrast, as the other model's parameters come into play, the drift exhibits a rather complicated dependence on the scaling exponent.

The paper is organized as follows. The model is described in section 2, which is a slight modification of the models previously studied in [14, 15]. Statistical properties of the model are briefly discussed in section 3. The characteristics of stationary drift, with numerical results, are presented in section 4. Conclusions and perspectives are offered in section 5.

2. Description of the model

In order to display the log-periodicity of the drift function of self-similar billiards discussed in section 4, which was predicted in [16], we will modify the self-similar billiard as defined earlier in [14, 15], and use a unit cell rather similar to the one obtained after conformal transformation of the iso-kinetic Lorentz channel [13]. In order to avoid further confusion, we pause to warn the reader that the analogy between our model and the iso-kinetic Lorentz channel does not go beyond this mere similarity. The dynamics are in fact very different, as will again be emphasized in the following.

The resulting cell has enhanced symmetry in that all the discs are now equivalent. The main motivation for introducing this modification is that it allows much greater values of the scaling parameter to be taken within the constraints imposed to guarantee ergodicity, see section 3.

In order to define the self-similar channel, we start with the description of the reference cell, examples of which are shown in figure 1.

We define the reference cell as the interior of a region bounded on the right and left sides by two arc-circles, with common centre and respective radii $\exp(\pm\epsilon/2)/\epsilon$ and, on the upper and lower sides, by two oblique lines of slopes $\pm \tan \sqrt{3}\epsilon/2^4$, with the exclusion of obstacles,

⁴ We note that these slopes may well be vertical and beyond when $\epsilon \geq \pi/\sqrt{3} \simeq 1.814$. This is not a restriction. Though ϵ could in principle be as large as $2\pi/\sqrt{3}$, we will see in section 3 that, for the sake of ergodicity, its maximal value is close to 2.

which are here taken to be regular discs. The parameter ϵ will henceforth be referred to as the *scaling exponent*, in contrast to the parameter μ which was defined in [14, 15] (or r in [16]), and which we refer to as the *scaling factor*, $\mu = \exp(\epsilon)$ ⁵.

Let the origin $(x, y) = (0, 0)$ be in the middle of the arc-circle of the left-hand side border. We have the central disc of radius ρ , located at

$$(x, y) = \left(\frac{1 - \exp(-\epsilon/2)}{\epsilon}, 0 \right),$$

two discs of radii $\rho \exp(-\epsilon/2)$ on the inner circle, at

$$\left(\frac{\exp(-\epsilon/2)}{\epsilon} [\cos(\sqrt{3}\epsilon/2) - 1], \pm \frac{\exp(-\epsilon/2)}{\epsilon} \sin(\sqrt{3}\epsilon/2) \right),$$

and two discs of radii $\rho \exp(\epsilon/2)$ on the outer circle, at

$$\left(\frac{\exp(\epsilon/2)}{\epsilon} \cos(\sqrt{3}\epsilon/2) - \frac{\exp(-\epsilon/2)}{\epsilon}, \pm \frac{\exp(\epsilon/2)}{\epsilon} \sin(\sqrt{3}\epsilon/2) \right).$$

Moreover, the corners where the boundaries of the cell intersect are located exactly at the centres of the outer discs.

Let \mathcal{D}_0 denote the reference cell. The extended system is obtained from the reference cell thus defined by making a copy of it, denoted by \mathcal{D}_1 , which we scale by a factor of $\exp(\epsilon)$ and attach to the right-hand side of the reference cell. Likewise, another copy of the reference cell, this time denoted by \mathcal{D}_{-1} , is scaled by $\exp(-\epsilon)$ and attached to its left-hand side. By repeating this procedure, copying and scaling the right- and left-most cells and attaching these copies to the existing sequence of cells, we obtain the self-similar Lorentz channel, which consists of an infinite collection $\{\mathcal{D}_n\}_{n \in \mathbb{Z}}$ of such cells. Obviously the usual Lorentz channel [3] is recovered for $\epsilon = 0$.

Note that when the value of ρ is large enough with respect to ϵ , the central circle of the reference cell \mathcal{D}_0 will intersect with its inner arc-circle border. Correspondingly a sixth disc appears in the reference cell, whose centre is located in cell \mathcal{D}_1 , to the right of the reference cell (as is the case in the examples shown in figure 1). This happens when $\rho \geq [1 - \exp(-\epsilon/2)]/\epsilon$.

A point-particle which moves in this extended system has unit speed and bounces off elastically when it collides with the scatterers and upper and lower walls. The circular walls which separate the cells from one another have no incidence on the dynamics. Taking into account the angle that the particle's velocity makes with the upper and lower walls at collisions, the reflection at these walls can be replaced by periodic boundary conditions, a modification which does not affect the radial motion. For special values of the scaling parameter, the corresponding self-similar billiard channel can be seen to span a self-similar billiard table, see figure 2.

As noticed in [14], the dynamics on the extended system can be boiled down to a single cell. Periodic boundary conditions, with rescaling of the arc-lengths and velocities, must then be imposed when trajectories collide on the circular sides to the right and left, reappearing on the opposite sides.

3. Ergodic properties

Although the geometry of the self-similar Lorentz channel is similar to that of the conformal transformation of the Gaussian iso-kinetic Lorentz gas, their dynamics are very different. By

⁵ The conformally transformed Gaussian iso-kinetic Lorentz channel has a similar cell geometry, but for the obstacles, which are deformed, slightly flattened, discs, see [13] for details. There the scaling exponent is given by the amplitude of the external forcing field.

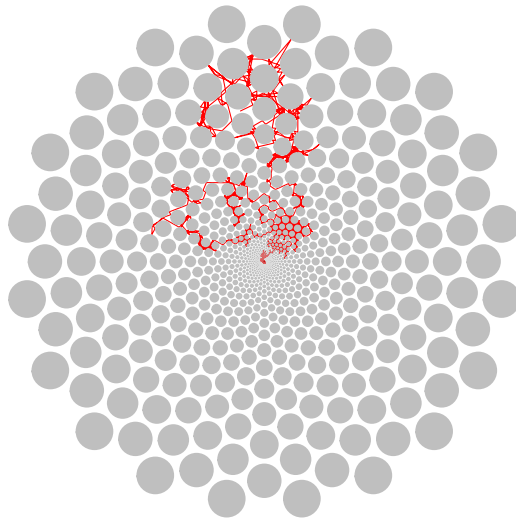


Figure 2. For values of $\epsilon = 2\pi/(n\sqrt{3})$, $n \geq 2$ integer, the angle between the upper and lower boundaries of the unit cell is $2\pi/n$. Consequently, the self-similar channel has a further symmetry, as it spans a self-similar table in the two-dimensional plane. The trajectory shown is that of a particle which moves in straight lines at unit speed and bounces off elastically when it collides with the scatterers. In this case, the drift velocity refers to the displacement along the radial component only. Here $n = 20$ is the number of discs per shell.

taking circular scatterers for all values of ϵ , we ensure that no transition to a non-hyperbolic regime will occur—see, e.g., chapter 4 of [5]. Nevertheless the similarities between the two lead to several immediate results regarding the ergodic properties of self-similar billiards restricted to the reference cell. We refer the reader to [16] for more details.

Two constraints have to be imposed on the parameter values, which have straightforward expressions in this geometry.

The first constraint is the finite horizon condition, by which we avoid the possibility that some trajectories may be ballistic. It is a straightforward generalization of the corresponding condition in the periodic Lorentz gas and here becomes

$$\rho > \rho_{\min} \equiv \frac{\sin(\sqrt{3}\epsilon/4)}{\epsilon}. \quad (1)$$

The second condition is that two discs on the same radius (with centre at $\exp(-\epsilon/2)/\epsilon$) do not overlap so that the cell remains connected,

$$\rho < \rho_{\max} \equiv \frac{1}{\epsilon} \frac{\exp(\epsilon) - 1}{\exp(\epsilon) + 1}. \quad (2)$$

The parameter values compatible with these two conditions are shown in figure 3.

4. Oscillations of the drift

Because of the biased geometry of the system, point-particles will preferentially move from small cells to large cells, i.e. from left to right, thus inducing a current of mass along the horizontal (radial) axis of the channel. Let $q(T)$ denote the displacement along this line after

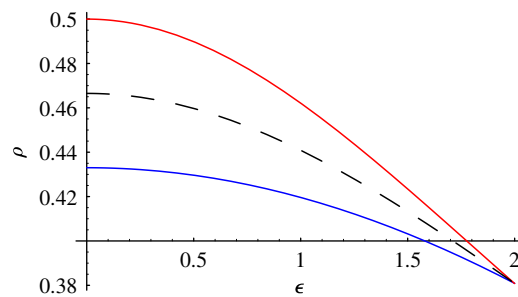


Figure 3. Allowed values of ρ versus ϵ from equations (1), $\rho \geq \rho_{\min}$ (bottom curve), and (2), $\rho \leq \rho_{\max}$ (upper curve). Ergodicity will not be guaranteed outside the domain bounded by these two curves. The dashed line indicates the line of parameters ρ_{mid} we use in the computations presented in section 4.

a time T . On average⁶, $q(T)$ grows linearly in T , which is to say, the current has a steady average value in time.

To be more precise, one can prove [16] that the ratio $q(T)/T$ remains of order one, in the sense that for any (small) $p > 0$ there are constants $0 < a < b < \infty$ such that $q(T)/T$ stays between a and b with probability $1 - p$. However, a detailed analysis [16] shows the current may actually retain a time dependence between those bounds.

The reason is that the probability distribution of the ratio $q(T)/T$ does not stabilize as $T \rightarrow \infty$; rather it keeps oscillating. This happens because the cell sizes grow exponentially; thus the size of the current cell (that is the cell where the particle is located at time T) is comparable to its entire previous displacement $q(T)$. To emphasize this effect, assume for a moment that the scaling factor between neighbouring cells is 2 (i.e. the scaling exponent $\epsilon = \ln 2$). Then the current cell would be just as big as all the previous cells combined. In other words, the geometric shape of the current cell scales up at the same rate as the particle's entire path.

This observation should convince the reader that the geometric structure of the current cell might affect the macroscopic evolution of $q(T)/T$. For example, there may be some parts of the cell which, on average, the particle traverses faster than others; in that case, as it passes through 'fast terrain', the ratio $q(T)/T$ would grow, and as it drags itself through 'slow motion areas', the ratio $q(T)/T$ would decrease. This happens periodically, as the particle moves from one cell to the next (even bigger) cell.

Note that the period of these oscillations is not fixed; it keeps growing exponentially with T . More precisely, the length of the period corresponds to the time it takes the particle to traverse the current cell completely, thus the ratio $q(T)/T$ versus $\log(T)/\epsilon$ should have period one.

These arguments were made precise in [16], where the following theorem was proved.

Theorem 1. Assume ϵ is chosen such that equations (1) and (2) are satisfied. The following holds. Let $\{T_n\}_{n \in \mathbb{N}}$ be a sequence of increasing times, $T_n \rightarrow \infty$, such that the fractional part of $\log T_n/\epsilon$ tends to a constant $0 \leq \delta < 1$. Then the distribution of $q(T_n)/T_n$ converges to a limit.

The theorem also implies that the limit of $q(T_n)/T_n$ may depend on the limiting fractional part of $\log T_n/\epsilon$, i.e. of δ . We may therefore expect that the ensemble-averaged quantity

⁶ Although the word average here refers to a time-average, we will usually reserve the word average to denote an ensemble average. Unless the context makes it clear, a quantity which is averaged with respect to time will be explicitly referred to as time-averaged.

Table 1. Different parameter values used in the numerical computations discussed below: ρ_{mid} in figures 4 and 5, and all three ρ_{min} , ρ_{mid} and ρ_{max} in figure 7.

ϵ	ρ_{min}	ρ_{mid}	ρ_{max}	ϵ	ρ_{min}	ρ_{mid}	ρ_{max}
0.1	0.432 877	0.466 231	0.499 584	1.1	0.416 824	0.435 921	0.455 018
0.2	0.432 472	0.465 406	0.498 34	1.2	0.413 789	0.430 665	0.447 541
0.3	0.431 796	0.464 04	0.496 283	1.3	0.410 504	0.425 125	0.439 746
0.4	0.430 851	0.462 145	0.493 438	1.4	0.406 974	0.419 333	0.431 691
0.5	0.429 638	0.459 738	0.489 837	1.5	0.403 202	0.413 317	0.423 433
0.6	0.428 158	0.456 839	0.485 521	1.6	0.399 194	0.407 108	0.415 023
0.7	0.426 413	0.453 475	0.480 536	1.7	0.394 952	0.400 732	0.406 511
0.8	0.424 404	0.449 67	0.474 936	1.8	0.390 483	0.394 213	0.397 943
0.9	0.422 135	0.445 456	0.468 777	1.9	0.385 79	0.387 575	0.389 36
1.0	0.419 607	0.440 862	0.462 117	1.997 65	0.380 998	0.380 998	0.380 998

$\langle q(T) \rangle / T$ will display oscillations as a function of $\log T / \epsilon$, with unit period. On the other hand, there may be no oscillations. Whether we can observe this oscillatory regime or not depends on the parameter values, as our numerical analysis reveals.

For the purpose of numerically demonstrating the drift oscillations, we let the scaling exponent ϵ vary between 0 and its maximal allowed value, near $\epsilon = 2$ (see figure 3), and take the corresponding radius to be either of ρ_{min} , equation (1), ρ_{max} , equation (2), or $\rho_{\text{mid}} \equiv 1/2(\rho_{\text{max}} + \rho_{\text{min}})$. The precise values of the parameters we used in our computations are shown in table 1.

Figure 4 shows the results of numerical computations of the drift function $\langle q(T) \rangle / T$ using up to 10^8 trajectories with random initial positions located on the central circle of cell \mathcal{D}_0 (or on the discs on the horizontal line when there is an overlap), and unit velocities at random angles. For each of these trajectories, we computed the horizontal position $q(T)$ at times T which we took to be logarithmically spaced on the interval $0 \leq \log T / \epsilon \leq 100$, so as to have 25 points on each unit interval of the scale $\log T / \epsilon$.

For values of the scaling exponent $\epsilon \gtrsim 1.0$, the regularity of the observed periodic oscillations is spectacular, as confirmed by the collapsed curves of figure 5. On the contrary, for values of $\epsilon \lesssim 0.8$ (only $\epsilon = 0.8$ is shown in figures 4 and 5), our measurements do not reveal the periodic oscillations predicted by theorem 1, which, in principle, applies to all values of ϵ .

The lack of noticeable periodic oscillations for small ϵ is due to a noise threshold, which is set by the number of trajectories used to measure the average drift. One must realize that the oscillations are a property of the average drift and not of single trajectories; the computation of the horizontal displacement of a single trajectory will reveal the tendency to move outwards and yield a good estimate of the time-averaged drift, but one needs to take ensemble averages in order to measure the log-periodic oscillations. This is illustrated in figure 6. The left panel shows the drift term $\langle q(T) \rangle / T$ averaged over different numbers of trajectories. The right panel shows the standard deviations to the asymptotic curve of each of these samples. One clearly sees the power-law decay of this quantity with the number of trajectories. Three different sets are shown, corresponding to different values of the scaling parameter; they all display the same decay, with an exponent value of about -1.15 .

The summary of our computational results is shown in figure 7, where the results corresponding to all three data sets listed in table 1 are compiled. The left-hand panel shows the average drifts as a function of ϵ , computed by taking the average of the time series of $\langle q(T) \rangle / T$. The right-hand panel shows the computed average amplitudes of the oscillations, which we denote by A , with the corresponding error bars. The amplitudes of the oscillations are here

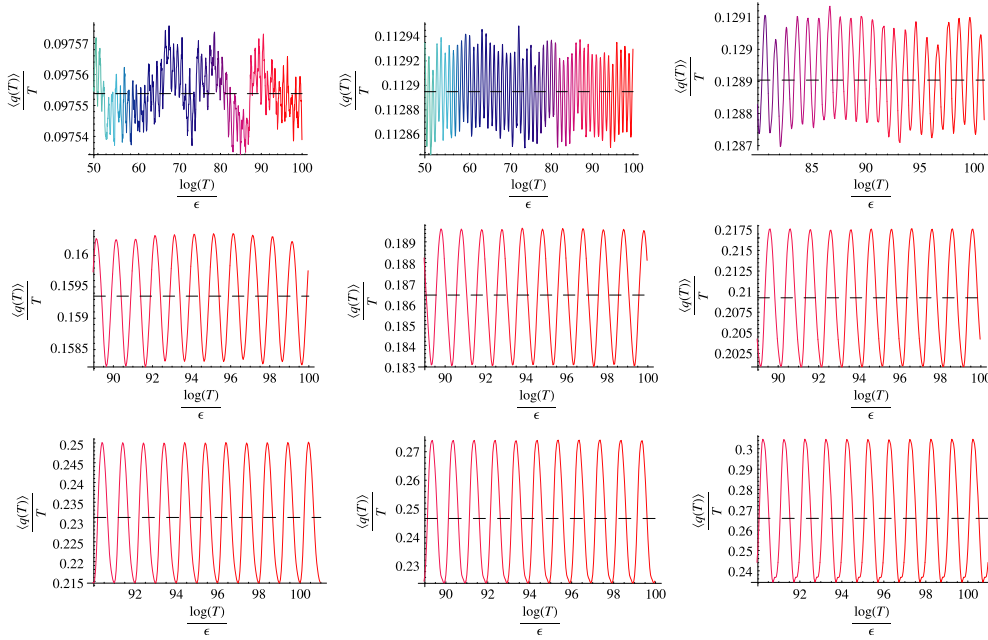


Figure 4. Average drift terms $\langle q(T) \rangle / T$ versus $\log(T) / \epsilon$. The parameter values of table 1 corresponding to $\rho = \rho_{\text{mid}}$ and $\epsilon = 0.8, 0.9, 1.0, 1.2, 1.4, 1.6, 1.8, 1.9$ and 1.99765 , in the order of increasing ϵ , left to right and top to bottom, are shown. The dashed lines show the computed time-averages, as plotted in figure 7. The number of trajectories used was 10^8 for the first two figures and 10^7 for all the others. The colour code is a hue, regularly varying from cyan to red as units of $\log T / \epsilon$ increase from 50 to 100. Note that the span of the x -axis was reduced for the larger ϵ values in order to better display the periodicity of the oscillations.

measured by taking the average of one-half of the sum of the minimum and maximum values of $\langle q(T) \rangle / T$ over each unit interval of $\log T / \epsilon$, which corresponds to a period of oscillation. Values of $\epsilon \leq 0.7$ were discarded, because oscillations could not be observed (yet).

The latter graph clearly demonstrates a power-law behaviour of the amplitude in the scaling factor, i.e. $A \sim \exp(a\epsilon)$, with the coefficient $a \simeq 1.5$, for parameter values $1.5 < \epsilon < 2.0$. The coefficient seems to be somewhat larger for smaller values of ϵ . The reason for this difference, we believe, is a non-trivial dependence in the parameter ρ , which here varies nonlinearly with ϵ . It might also be due to our limited statistics (as also reflected by the large error bars).

Comparing figures 6 and 7, the reader will appreciate that oscillations of amplitudes down to $\mathcal{O}(10^{-5})$ were measured about a drift value of $\mathcal{O}(10^{-1})$. Distinct oscillations become faint as the ratio between their amplitudes, shown on the right panel of figure 7, and the standard deviations to the asymptotic curve, shown on the right panel of figure 6, decrease to ≈ 1 and below. One wishes to increase this ratio and reduce the noise threshold in order to measure drift oscillations for smaller values of the scaling parameter. This can be achieved by increasing the number of trajectories. Unfortunately the required cpu time quickly grows beyond manageable levels.

5. Concluding remarks

To conclude, self-similar billiard channels are instances of non-equilibrium chaotic billiards with volume-preserving dynamics, whereby a geometric constraint induces a current of mass,

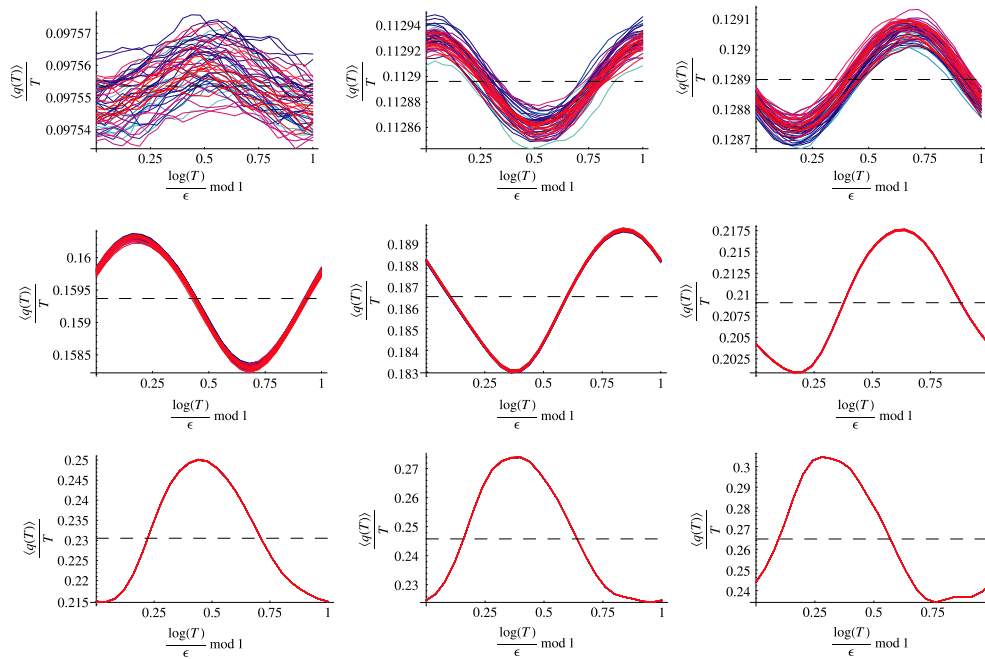


Figure 5. Same as figure 4 with the horizontal axis taken modulo 1. For every figure, we plot the last 50 oscillations. The colour code is identical to figure 4. When ϵ is large enough, the curves nicely collapse on the same periodic function.

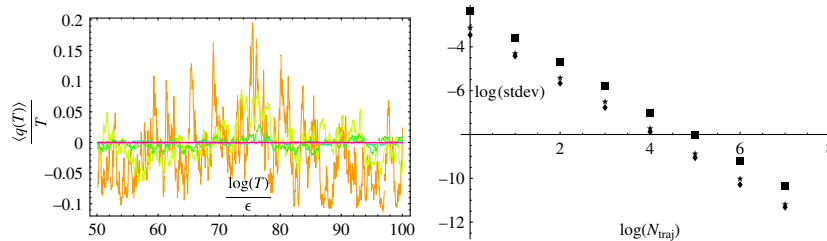


Figure 6. (Left panel) Average drift term $\langle q(T) \rangle / T$ versus $\log(T) / \epsilon$ for data sets of sizes 10^n trajectories, $n = 0, 1, \dots, 8$. Here $\epsilon = 0.9$ and $\rho = \rho_{\text{mid}}$. The deviations to the asymptotic curve do not decay with time; they remain constant and can be so large as to hide the underlying drift oscillations when the number of trajectories is not large enough. (Right panel) Standard deviations in the computation of the average drift term versus the number of trajectories, $\epsilon = 1.9$ (squares), 1.0 (pluses), 0.9 (diamonds). The power-law decay is about -1.15 for all three sets.

going from the smaller to the larger scales. The paper clearly establishes the following novel results:

- (i) When the scaling exponent is large enough, log-periodic drift oscillations do occur, which is to say that the ensemble-averaged drift is not constant in time, even though its time-averaged value is well-defined.
- (ii) As the scaling exponent becomes small, the time-averaged drift decreases linearly with it and becomes much larger than the amplitudes of its oscillations, thus making the latter harder to detect.

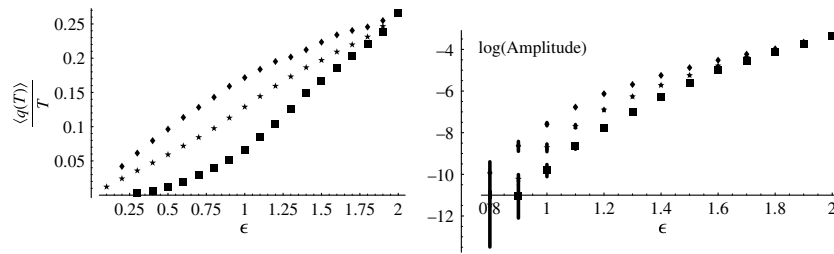


Figure 7. Time-averaged drifts (left) and oscillation amplitudes (right) measured for the parameter values of table 1, ρ_{\min} (diamonds), ρ_{mid} (plus), ρ_{\max} (squares). For small ϵ , the oscillation amplitudes decrease below the noise threshold, hence the larger error bars at $\epsilon = 0.8$.

- (iii) The amplitudes of the oscillations follow a power law in the scaling factor, more clearly so for the larger range of parameter values.

Our results further establish how the noise to signal ratio hinders the measurement of distinct drift oscillations as the size of the ensemble averages vary. In this respect, a useful direction for future research, which is beyond the scope of this paper, would be to give a theoretical estimate for the behaviour of the oscillations' amplitudes as $\epsilon \rightarrow 0$.

We further emphasize that our results do not just confirm the results presented in [16], but actually extend them. Theorem 1 says that the linear growth of the average displacement is periodic in time, but that does not necessarily imply that this function has periodic oscillations. In fact, a constant function is also periodic (with any period). The theorem proved in [16] leaves open the possibility that the function be either periodic (with a definite period) or constant. We have here resolved this alternative by numerically demonstrating that the linear growth of the average displacement is in fact truly periodic, with a definite period. We thus discover that the first of the alternative (and mutually exclusive) results of theorem 1 actually takes place, which is an interesting and unusual property. This is the main achievement of this paper.

It is to be noted that property (i) is an expected consequence of the discrete scale invariance of the system, which typically manifests itself in the presence of power laws with complex exponents. The signature of such power laws are the log-periodic corrections to their scalings, in this case the corrections to $q(T) \sim T$. Similar phenomena are observed in many different physical situations, see [17] and references therein. That the drift oscillations are barely noticeable when the scaling exponent decreases below $\epsilon = 1.0$ is perhaps not surprising as log-periodicity is typically a very small effect. Going to the other end of the parameter range, it is actually remarkable that the regularity of drift oscillations is so well pronounced for larger values of ϵ . In this regard, self-similar billiards offer new ground for further studies of this interesting phenomenon, here in the framework of hyperbolic dynamical systems, and thus improve our understanding of a ubiquitous property which has already found many known fields of application.

Acknowledgments

The authors wish to thank D Dolgopyat for helpful comments. FB acknowledges financial support from the Fondecyt Project 1060820 and FONDAP 11980002 and Anillo ACT 15. NC is partially supported by the NSF Grant DMS-0354775. TG is financially supported by the Fonds National de la Recherche Scientifique.

References

- [1] Hoover W G 2001 *Time Reversibility, Computer Simulation, and Chaos* (Singapore: World Scientific)
- [2] Evans D J and Morriss G P 1990 *Statistical Mechanics of Non-Equilibrium Fluids* (London: Academic)
- [3] Gaspard P 1998 *Chaos, Scattering and Statistical Mechanics* (Cambridge: Cambridge University Press)
- [4] Dorfman J R 1999 *An Introduction to Chaos in Nonequilibrium Statistical Mechanics* (Cambridge: Cambridge University Press)
- [5] Chernov N I and Markarian R 2006 *Chaotic Billiards (Mathematical Surveys and Monographs vol 127)* (Providence, RI: American Mathematical Society)
- [6] Bunimovich L A, Sinai Ya G and Chernov N I 1991 Statistical properties of two-dimensional hyperbolic billiards *Russ. Math. Surv.* **46** 47
- [7] Gaspard P, Claus I, Gilbert T and Dorfman J R 2001 The fractality of the hydrodynamic modes of diffusion *Phys. Rev. Lett.* **86** 1506
- [8] Gaspard P 1997 Chaos and hydrodynamics *Physica A* **240** 54
- [9] Chernov N I, Eyink G L, Lebowitz J L and Sinai Ya G 1993 Derivation of Ohm's law in a deterministic mechanical model *Phys. Rev. Lett.* **70** 2209
Chernov N I, Eyink G L, Lebowitz J L and Sinai Ya G 1993 Steady state electric conductivity in the periodic Lorentz gas *Commun. Math. Phys.* **154** 569
- [10] Ruelle D 1996 Positivity of entropy production in non-equilibrium statistical mechanics *J. Stat. Phys.* **85** 1
Ruelle D 2003 Extending the definition of entropy to non-equilibrium steady states *Proc. Natl Acad. Sci.* **100** 30054
- [11] Dettmann C P and Morriss G P 1996 Hamiltonian formulation of the Gaussian iso-kinetic thermostat *Phys. Rev. E* **54** 2495
Morriss G P and Dettmann C P 1998 Thermostats: analysis and application *Chaos* **8** 321
- [12] Wojtkowski M P 2000 W-flows on Weyl manifolds and Gaussian thermostats *J. Math. Pures Appl.* **79** 953
- [13] Barra F and Gilbert T 2007 Non-equilibrium Lorentz gas on a curved space *J. Stat. Mech.* **7** L01003
- [14] Barra F, Gilbert T and Romo M 2006 Drift of particles in self-similar systems and its Liouvillian interpretation *Phys. Rev. E* **73** 026211
- [15] Barra F and Gilbert T 2007 Steady-state conduction in self-similar billiards *Phys. Rev. Lett.* **98** 130601
- [16] Chernov N and Dolgopyat D 2007 Particle's drift in self-similar billiards *Preprint*
- [17] Sornette D 1998 Discrete scale invariance and complex dimensions *Phys. Rep.* **297** 239